Non-Destructive Testing of Non-Metallic Concentric Pipes Using Microwave Measurements

Hailun Wu¹, Maryam Ravan², Raveena Sharma³, Jay Patel⁴, and Reza K. Amineh⁵
Applied Electromagnetics Research Lab, New York Institute of Technology, USA

¹hwu28@nyit.edu, ²mravan@nyit.edu, ³rsharm22@nyit.edu, ⁴jpate197@nyit.edu, ⁵rkhalaja@nyit.edu

Abstract—Recently, non-metallic materials which are resilient-to-corrosion, low cost, and light weight have been exploited in many industrial sectors. A common application of them is in the form of pipes. Due to the fact that the traditional NDT methods are mostly effective for metallic pipes, here, a microwave holographic imaging combined with standardized minimum norm (SMN) is proposed for inspection of multiple concentric non-metallic pipes. To reduce the complexity of the system, we aim at using the narrowest possible frequency band by using an array of receiver antennas. The validity of the proposed imaging method is demonstrated via simulation and experimental results.

Keywords—microwave imaging, non-destructive testing (NDT), non-metallic pipes, standardized minimum norm (SMN).

I. INTRODUCTION

Non-metallic and composite components are commonly used in various industrial sectors due to their significant advantages, such as resilience to corrosion, light weight, and cost efficiency. Thus, robust and reliable non-destructive testing (NDT) methods for these materials are in demand to allow their widespread use in critical applications.

Recently, to address the above-mentioned requirement, microwave measurements have been proposed (e.g., see [1]). In [2]-[5], two dimensional (2D) imaging has been performed using scalar measurements only. In [6], a K-band (18 GHz – 26.5 GHz) microwave reflectometry system employing an inline crawling robot has been proposed. In [7], wideband millimetre wave synthetic aperture radar (SAR) imaging technique has been employed to produce three-dimensional (3D) images of vertical cracks in flat and curved single pipes.

In this paper, a holographic microwave imaging technique is proposed to provide images of multiple concentric pipes. Such configuration is commonly used in various industries to increase the lifetime of the pipeline [8] or to separate the flow in the fluid transfer pipeline [9]. To reduce the complexity and the cost, we aim at using the narrowest possible frequency band by using an array of antennas. This also reduces the imaging errors due to the dispersive properties of the media and the data acquisition time. The conventional minimum norm (MN) solution process in microwave holographic imaging is augmented by using standardized minimum norm (SMN) approach. This alleviates depth biasing problem associated with MN approach, i.e., underestimation of deep features in favor of ones that are more superficial.

II. THEORY

Here, we first review the theory of near-field holographic imaging with an array of receiver antennas for imaging nonmetallic concentric pipes. We then propose the SMN approach to augment the solution process.

A. Holographic Microwave Imaging

Fig. 1 illustrates the proposed microwave imaging setup including a transmitter antenna to illuminate pipes and an array of N_A receiver antennas that scans the scattered fields. The transmitter antenna and the array of receiver antennas scan a cylindrical aperture with radius of r_A and height of z_A . The scattered field is recorded at N_{ϕ} angles along the azimuthal direction ϕ (within $[0,2\pi]$) and N_z positions along the longitudinal direction z. The complex-valued scattered field $E^{SC}(\phi,z)$ is measured, at each sampling position, at N_{ϕ} frequencies within the band of ω_1 to ω_{N_n} , by each receiver. Such scattered response is obtained from subtracting the response of the pipes without defects from the response of the same pipes with defects. The image reconstruction process then provides images of the pipes with radii r_i , where $i = 1, ..., N_r$. It is worth noting that the imaging system is assumed to be linear and space-invariant (LSI). The use of Born approximation for the scattering integral leads to the linear property of the imaging system (e.g., see [10]).

For implementation of the holographic imaging, first, the point-spread functions (PSFs) of the LSI imaging system are acquired. These PSFs are approximated by measuring small defects called calibration defects (CDs) placed on each pipe one at a time. These CDs are the smallest defects that can be measured by the system. To provide more data for image

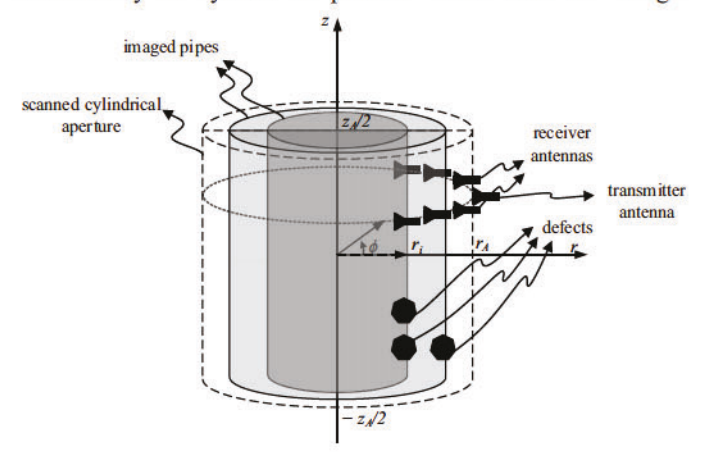


Fig. 1. Illustration of the microwave imaging setup.

reconstcrution, measurements can be implemented at multiple frequencies (over the narrowest possible band), ω_n , $n=1,\ldots,N_{\omega}$ and by multiple receivers, a_m , $m=1,\ldots,N_{\Delta}$. We denote the measured PSF function for the *i*-th pipe measured by the receiver antenna a_m at frequency ω_n by $E_{i,a_m}^{SC,CD}(\phi,z,\omega_n)$. We also denote the measured scattered field by the receiver antenna a_m at frequency ω_n by $E_{a_m}^{SC}(\phi,z,\omega_n)$. Let's first consider the spatially-sampled versions of $E_{a_m}^{SC}(\phi,z,\omega_n)$, $E_{i,a_m}^{SC,CD}(\phi,z,\omega_n)$, and $f_i(\phi,z)$ denoted by $\mathbf{E}_{a_m}^{SC}(n_\phi,n_z,\omega_n)$, $\mathbf{E}_{i,a_m}^{SC,CD}(n_\phi,n_z,\omega_n)$, and $\mathbf{f}_i(n_\phi,n_z)$. Here, Using the convolution theory, discrete Fourier transforms (DFT) along ϕ direction, and discrete time FT (DTFT) along z direction, it can be shown that the contrast functions of the defects on the pipes $f_i(\phi,z)$, $i=1,\ldots,N_r$, can be found by solving the following system of equations at each spatial frequency pair $\mathbf{K}=(k_\phi,k_z)$ [10][11]:

$$\frac{\tilde{\mathbf{E}}^{SC}}{\mathbf{E}} = \frac{\tilde{\mathbf{D}}\tilde{\mathbf{F}}}{\mathbf{E}} \tag{1}$$

where

$$\underline{\underline{\tilde{\mathbf{E}}}}^{SC} = \begin{bmatrix} \underline{\underline{\tilde{\mathbf{E}}}}_{1}^{SC} \\ \vdots \\ \underline{\underline{\tilde{\mathbf{E}}}}_{N_{A}}^{SC} \end{bmatrix}, \ \underline{\underline{\tilde{\mathbf{D}}}} = \begin{bmatrix} \underline{\tilde{\mathbf{D}}}_{1} \\ \vdots \\ \underline{\tilde{\mathbf{D}}}_{N_{A}} \end{bmatrix}, \ \underline{\underline{\tilde{\mathbf{F}}}} = \begin{bmatrix} \underline{\tilde{\mathbf{f}}}_{1}(\boldsymbol{\kappa}') \\ \vdots \\ \underline{\tilde{\mathbf{f}}}_{N_{r}}(\boldsymbol{\kappa}') \end{bmatrix}$$
(2)

and

$$\underline{\underline{\tilde{\mathbf{E}}}}_{a_m}^{SC} = \begin{bmatrix}
\tilde{\mathbf{E}}_{a_m}^{SC}(\boldsymbol{\kappa}, \omega_{l}) \\
\vdots \\
\tilde{\mathbf{E}}_{a_m}^{SC}(\boldsymbol{\kappa}, \omega_{N_{\omega}})
\end{bmatrix},$$

$$\underline{\underline{\tilde{\mathbf{D}}}}_{a_m} = \begin{bmatrix}
\tilde{\mathbf{E}}_{1,a_m}^{SC,CD}(\boldsymbol{\kappa}, \omega_{l}) & \cdots & \tilde{\mathbf{E}}_{N_r,a_m}^{SC,CD}(\boldsymbol{\kappa}, \omega_{l}) \\
\vdots & \ddots & \vdots \\
\tilde{\mathbf{E}}_{1,a_m}^{SC,CD}(\boldsymbol{\kappa}, \omega_{N_{\omega}}) & \cdots & \tilde{\mathbf{E}}_{N_r,a_m}^{SC,CD}(\boldsymbol{\kappa}, \omega_{N_{\omega}})
\end{bmatrix}$$
(3)

where $\tilde{\mathbf{E}}_{a_m}^{SC}(\mathbf{K},\omega_n)$, $\tilde{\mathbf{E}}_{i,a_m}^{SC,CD}(\mathbf{K},\omega_n)$, and $\tilde{\mathbf{f}}_i(\mathbf{K})$ denotes DFT along ϕ axis and DTFT along z axis of $\mathbf{E}_{a_m}^{SC}(n_\phi,n_z,\omega_n)$, $\mathbf{E}_{i,a_m}^{SC,CD}(n_\phi,n_z,\omega_n)$, and $\mathbf{f}_i(n_\phi,n_z)$, respectively. These systems of equations are solved at each $\mathbf{K}=(k_\phi,k_z)$ pair to obtain the values for $\tilde{\mathbf{f}}_i(\mathbf{K})$, $i=1,\ldots,N_r$. Then, inverse DTFT along z and inverse DFT along ϕ are applied to reconstruct images $\mathbf{f}_i(n_\phi,n_z)$ over all the pipes with radii $r=r_i$, $i=1,\ldots,N_r$. At the end, the normalized modulus of $\mathbf{f}_i(n_\phi,n_z)$, $|\mathbf{f}_i(n_\phi,n_z)|/M$, where M is the maximum of $|\mathbf{f}_i(n_\phi,n_z)|$ for all r_i , is plotted to obtain a 2D image of the defects on the i-th pipe. We call $|\mathbf{f}_i(n_\phi,n_z)|/M$ the normalized image.

B. Using Standardized Minimum Norm Approach
 The common approach to solve the systems of equations in

near-field holographic imaging is the well-known MN solution [10][11]. However, in the MN estimations, the solution is harmonic in nature, which implies the Laplacian of the solution is zero. Thus, it produces a smooth solution [12]. As a result, the deep defects are not properly localized on the right pipe. In other words, this leads to only detection of the defects that are closer to the antennas. Thus, inspired by standardized low-resolution brain electromagnetic tomography using EEG data [12], we study the improvements gained via SMN of the inverse solution by standardizing of the contrast function.

First, the cost function to be minimized is constructed as:

$$J = \left\| \underline{\underline{\tilde{\mathbf{E}}}}^{SC} - \underline{\tilde{\mathbf{D}}}\underline{\tilde{\mathbf{F}}} \right\|^{2} + \alpha \left\| \underline{\underline{\tilde{\mathbf{F}}}} \right\|^{2}$$
 (4)

where $\|\cdot\|$ is the 2-norm operator and $\alpha \ge 0$ is a regularization parameter. This parameter is taken as the variance of the noise in the simulated or measured data. The functional J is to be minimized with respect to $\tilde{\mathbf{F}}$, for given $\tilde{\mathbf{D}}$, $\tilde{\mathbf{E}}^{SC}$, and α . The explicit solution to this minimization problem is:

$$\frac{\widetilde{\widetilde{\mathbf{F}}}}{\widetilde{\mathbf{F}}} = \mathbf{P} \widetilde{\underline{\widetilde{\mathbf{F}}}}^{SC} \tag{5}$$

where

$$\mathbf{P} = \underline{\underline{\tilde{\mathbf{D}}}}^{\mathsf{H}} \mathbf{L} \left[\mathbf{L} \underline{\underline{\tilde{\mathbf{D}}}} \underline{\underline{\tilde{\mathbf{D}}}}^{\mathsf{H}} \mathbf{L} + \alpha \mathbf{L} \right]^{\dagger} , \qquad (6)$$

 $\underline{\tilde{\mathbf{F}}}$ is the estimate of $\underline{\tilde{\mathbf{F}}}$, $\mathbf{L}_{N_\omega N_A \times N_\omega N_A} = \mathbf{I} - \mathbf{1} \mathbf{1}^{\mathrm{T}} \mathbf{1}$ denotes the centering matrix, $\mathbf{I}_{N_\omega N_A \times N_\omega N_A}$ is the identity matrix, $\mathbf{1}_{N_\omega N_A \times 1}$ is a vector of ones, $[\cdot]^{\mathrm{H}}$ is Hermitian transpose operation, and $[\cdot]^{\dagger}$ denotes Moore-Penrose pseudoinverse. Standardization of the estimate $\widehat{\underline{\tilde{\mathbf{F}}}}$ requires an estimate of its variance. The true variance of $\underline{\tilde{\mathbf{F}}}$ is equal to the identity matrix but this is for an ideal case when $\underline{\tilde{\mathbf{F}}}$ is estimated without error. Thus, in reality, to obtain variance of $\widehat{\underline{\tilde{\mathbf{F}}}}$ denoted by $\mathbf{S}_{\underline{\tilde{\mathbf{F}}}}$, from (5), we have:

$$\mathbf{S}_{\hat{\mathbf{E}}} = \mathbf{P} \mathbf{S}_{\hat{\mathbf{E}}^{SC}} \mathbf{P}^{H} \tag{7}$$

where $\mathbf{S}_{\underline{\tilde{\mathbf{E}}}^{SC}}$ is the variance of $\underline{\tilde{\mathbf{E}}}^{SC}$ from the Bayesian point of view and it is due to the noisy measurements. Assuming independence of $\underline{\tilde{\mathbf{F}}}$ and measurement noise, $\mathbf{S}_{\underline{\tilde{\mathbf{E}}}^{SC}}$ can be written as:

$$\mathbf{S}_{\underline{\tilde{\mathbf{E}}}^{SC}} = \underline{\underline{\tilde{\mathbf{D}}}} \underline{\underline{\tilde{\mathbf{D}}}}^{H} + \mathbf{S}_{\underline{\tilde{\mathbf{E}}}^{SC}}^{noise} = \underline{\underline{\tilde{\mathbf{D}}}} \underline{\underline{\tilde{\mathbf{D}}}}^{H} + \alpha \mathbf{L}$$
 (8)

Therefore, from (7) and (8), the variance of $\hat{\tilde{\mathbf{F}}}$ is

$$\mathbf{S}_{\frac{\hat{\mathbf{p}}}{\mathbf{F}}} = \mathbf{P} \left(\underline{\underline{\tilde{\mathbf{p}}}} \underline{\underline{\tilde{\mathbf{p}}}} \underline{\tilde{\mathbf{p}}}^{\mathbf{H}} + \alpha \mathbf{L} \right) \mathbf{P}^{\mathbf{H}} = \underline{\underline{\tilde{\mathbf{p}}}}^{\mathbf{H}} \left(\underline{\underline{\tilde{\mathbf{p}}}} \underline{\underline{\tilde{\mathbf{p}}}} \underline{\tilde{\mathbf{p}}}^{\mathbf{H}} + \alpha \mathbf{L} \right)^{+} \underline{\underline{\tilde{\mathbf{p}}}}$$
(9)

The standardization of $\hat{\tilde{\mathbf{F}}}$ is then estimated as [13]:

$$\frac{\hat{\underline{\tilde{E}}}}{\tilde{\underline{F}}} = \sqrt{(\text{Diag}(S_{\frac{\tilde{E}}{F}}))^{-1}} P \frac{\tilde{\underline{E}}^{SC}}{\tilde{\underline{E}}}$$
(10)

where ${\rm Diag}(S_{\frac{2}{k}})$ is the diagonal matrix formed by the diagonal elements of $S_{\frac{2}{k}}$.

III. SIMULATION RESULTS

In a FEKO simulation setup shown in Fig. 2, we use an array of 13 dipole antennas for imaging double concentric pipes. Table I shows the values of the parameters in Fig. 2. The center element is excited while the rest of the antennas are used as the receivers. There are two semi-cylindrical defects on the outer pipe with angular separation $\Delta \phi_d = 20^\circ$ and one defect with the same shape and size on the inner cylinder centered at $\phi = 0^\circ$. The pipes have a relative permittivity ε_r of 2.25 and loss tangent of 0.0004.

The complex-valued S-parameters are obtained every 2° by rotating the antenna(s) along the azimuth angle (ϕ). To have a realistic simulation study, additive White Gaussian noise with signal-to-noise ratio (SNR) of 20 dB is applied.

Then, holographic imaging is applied on the scattered responses. Fig. 3 shows the reconstructed images for the pipes. It is observed that when using holographic imaging with SMN approach compared to MN approach, the quality of the reconstructed images drastically improves, in particular, for the inner pipe as expected. We can clearly detect the defects at their true locations on both pipes after applying holographic imaging with SMN approach. We evaluate the resolutions of the images in the ϕ direction in terms of the distance between two points marking 0.7 times the peak value. They are found to be approximately 4.8 mm and 3.4 mm for the outer and inner pipes, respectively.

IV. EXPERIMENTAL RESULTS

In this section, in order to validate the proposed imaging technique, we conduct proof-of-concept experiments.

For imaging the pipes, a cavity-backed printed spiral antenna is designed and fabricated. The antenna is designed in FEKO software with the target frequency of 6 GHz to 8 GHz. This frequency band allows for: (1) imaging cylindrical surfaces (pipes) with a separation of approximately 11 mm which is suitable, in practice, for standard pipes, (2) cost-effective data acquisition systems, (3) operating within ultrawide band (UWB) frequency range approved by federal communication commission (FCC) for unlicensed low power applications, and (4) inspection of pipes which may carry lossy fluids. For brevity, here, we skip the details of designing the antennas.

The transmitter antenna and the array of receiver antennas are placed inside a holder made by 3D printing and in a configuration similar to the simulation model in Fig. 2, i.e., the angular separation of the antennas is $\Delta \phi_a = 20^{\circ}$ and the transmitter antenna is placed in the middle. The antennas are connected to an RF SP8T switch (EV1HMC321ALP4E from Analog Devices operating up to 8 GHz). The RF switch is connected to an Arduino Uno board which can be controlled via MATLAB. We constructed a cylindrical scanning system moving along ϕ and z. The antennas scan double concentric

PVC pipes placed inside the antenna holder. Fig. 4 shows the complete imaging setup. At each sampling step, the complex-valued S parameters are measured via an Anritsu MS46122B vector network analyzer (VNA). The data acquisition including switching between receiver antennas as well as the control of the scanning system is implemented via MATLAB.

In the experiment, PVC pipes with the outer diameters of 152.4 mm (6 inch) and 101.6 mm (4 inch) are employed. The inner pipe has a thickness of 7 mm while the outer one has a thickness of 5 mm. Circular defects with diameters of 55 mm are made on the pipes. In the test scenario, two defects are on the outer pipe at $(\phi,z) = (\pm 90^{\circ}, 0)$ and one defect is on the inner pipe at $(\phi,z) = (0^{\circ}, 0)$. The PSFs and responses of the test scenario are collected over cylindrical aperture with radius of 152.4 mm and height of 240 mm with sampling steps of every

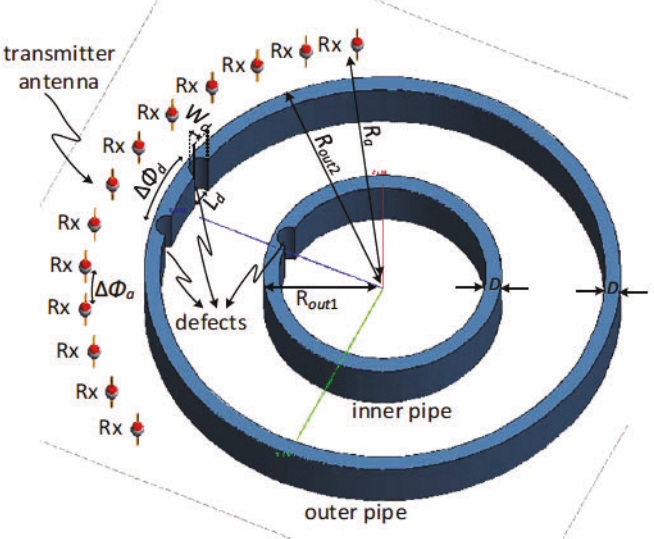
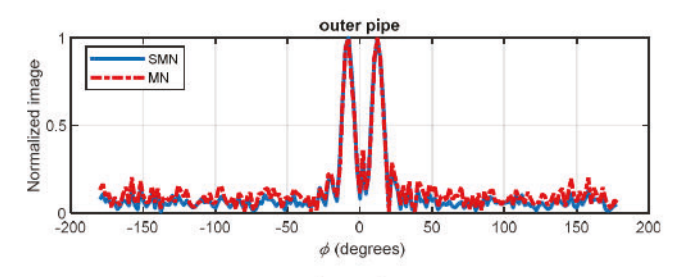


Fig. 2. Illustration of the FEKO simulation setup.

Table 1. Parameter values for the setup in Fig. 2.

N_A	$\Delta \phi_a$	Ra	Rout1	Rout2	D	L_d	W_d	$\Delta \phi_d$
12	10°	50 mm	20 mm	40 mm	2 mm	1.5D	0.75D	20°



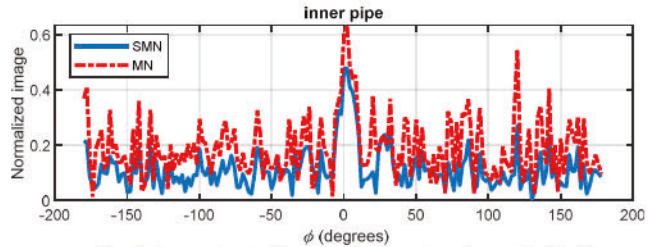


Fig. 3. Reconstructed images for the setup shown in Fig. 2.

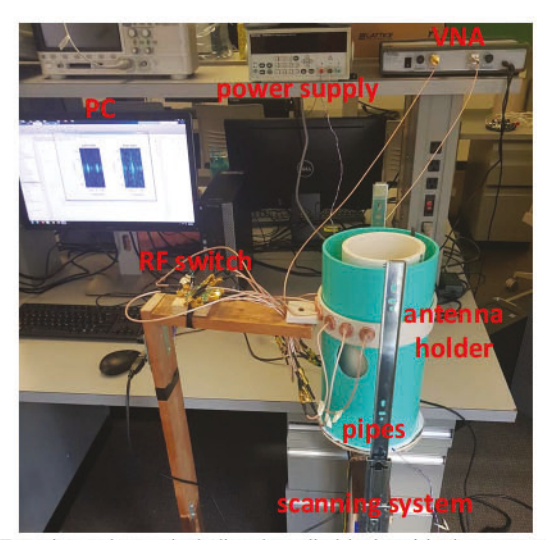


Fig. 4. Experimental setup including the cylindrical positioning system, double concentric PVC pipes, a transmitter antenna, an array of receiver antennas, VNA, RF switch, power supply, and PC.

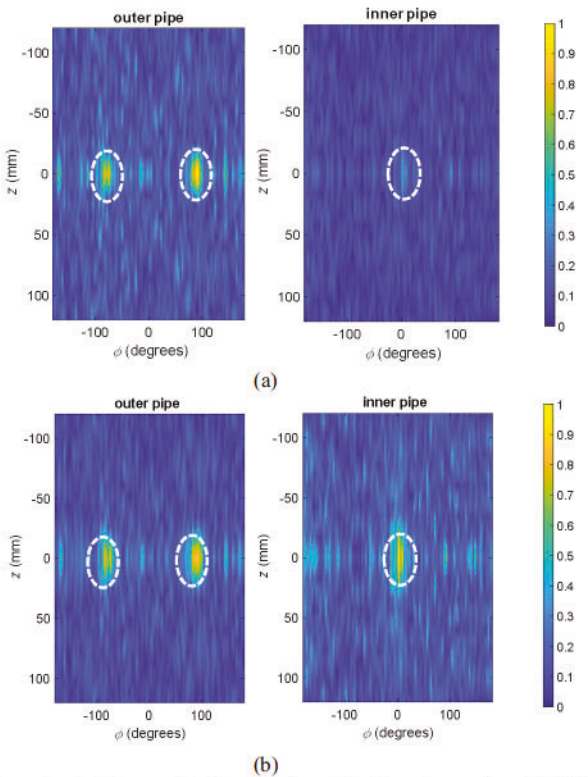


Fig. 5. Reconstructed images for the experimental setup when using: (a) MN approach using 10 frequencies and (b) SMN approach using 10 frequencies.

3.6° and 8 mm over the band of 6 GHz to 8 GHz.

We employ 10 frequencies within the above-mentioned band for image reconstruction. After applying the holographic imaging with MN approach and with SMN approach to the experimental data collected by eight receiver antennas, reconstructed images of the pipes are obtained. Fig. 5(a) shows the reconstructed images using MN approach. It is observed that two defects on the outer pipe can be reconstructed while the one on the inner pipe cannot be distinguished well. Fig. 5(b)

shows the reconstructed images using SMN approach. Compared to Fig. 5(a), it is observed that the defect on the inner pipe can also be reconstructed well.

V. CONCLUSION

In this paper, we proposed an NDT technique for imaging non-metallic concentric non-metallic pipes. It is based on microwave holographic imaging augmented by an SMN approach for solving the systems of equations.

The performance of the proposed imaging technique is demonstrated via simulation and experimental results. It was observed that using SMN approach significantly enhances the quality of the reconstructed images of the defects on the pipes.

The imaging technique is based on DFT, DTFT, and solution of small systems of equations. This makes the technique fast and robust. The use of such NDT technique promotes the use of emerging non-metallic pipes in critical industrial sectors.

ACKNOWLEDGMENT

This project has been supported by US national science foundation (NSF), award No. 1920098, and New York Institute of Technology's (NYIT) Institutional Support for Research and Creativity (ISRC) Grants.

REFERENCES

- R. Zoughi, Microwave Non-Destructive Testing and Evaluation. Kluwer Academic Publishers, 2000.
- [2] R. J. Stakenborghs, "Microwave inspection method and its application to FRP," MTI AmeriTAC 110 Conf. (MTI AmeriTAC), 2013.
- [3] R. Stakenborghs, "Microwave based NDE inspection of HDPE pipe welds," 17th Int. Conf. on Nuclear Engineering ICONE17, 2009.
- [4] K. Schmidt, T. Aljundi, G. A. Subaii, and J. Little, "Microwave interference scanning inspection of nonmetallic pipes," 5th Middle East Nondestructive Testing Conf. & Exhibition, Manama, Bahrain 2009.
- [5] D. M. Tripathi, S. Gunasekaran, S. S. Murugan, and N. A. Enezi, "NDT by microwave test method for non metallic component," *Indian National Seminar & Exhibition on Non-Destructive Evaluation NDE*, 2016.
- [6] T. D. Carrigan, B. E. Forrest, H. N. Andem, K. Gui, L. Johnson, J. E. Hibbert, B. Lennox, and R. Sloan, "Nondestructive testing of nonmetallic pipelines using microwave reflectometry on an in-line inspection robot," *IEEE Trans. Inst. Meas.*, vol. 68, no. 2, pp. 586–594, Feb. 2019.
 [7] M. T. Ghasr, K. Ying, and R. Zoughi, "3D millimeter wave imaging of
- [7] M. T. Ghasr, K. Ying, and R. Zoughi, "3D millimeter wave imaging of vertical cracks and its application for the inspection of HDPE pipes," *AIP Conf. Proc.*, vol. 1581, no. 1, pp. 1531–1536, 2014.
- [8] L. E. S. Martin, A. E. Fouda, R. K. Amineh, I. Capoglu, B. Donderici, S. S. Roy, F. Hill, "New high-definition frequency tool for tubing and multiple casing corrosion detection," SPE Abu Dhabi Int. Petroleum Exhibition & Conference, 2017.
- [9] Y. Renardy, D. D. Joseph, "Couette flow of two fluids between concentric pipes," J. of Fluid Mechanics, vol. 150, pp. 381–394, Jan. 1985.
- [10] R. K. Amineh, N. K. Nikolova, and M. Ravan, Real-Time Three-Dimensional Imaging of Dielectric Bodies Using Microwave/Millimeter Wave Holography. Wiley & IEEE Press, ISBN: 978-1-119-53886-8, 2019.
- [11] H. Wu and R. K. Amineh, "A low-cost and compact three-dimensional microwave holographic imaging system," *Electronics*, vol. 8, no. 9, 2019.
- [12] R. D. Pascual-Marqui, "Standardized low resolution brain electromagnetic tomography (sLORETA): technical details," *Methods Find. Exp. Clin. Pharmacol.*, vol. 24, suppl D:5-12, pp. 1–16, 2002.
- [13] A. M. Dale, A. K. Liu, B. R. Fischl, R. L. Buckner, J. W. Belliveau, J. D. Lewine, and E. Halgren, "Dynamic statistical parametric mapping: combining fMRI and MEG for highresolution imaging of cortical activity," *Neuron*, vol. 26, pp. 55-67, 2000.